applied optics

Idler-efficiency-enhanced long-wave infrared beam generation using aperiodic orientation-patterned GaAs gratings

Ziya Gürkan Figen,[1] Orhan Aytür,[2] and Orhan Arikan[2]

[1]TÜBİTAK BİLGEM/İLTAREN, 06800 Ümitköy, Ankara, Turkey
[2]Department of Electrical and Electronics Engineering, Bilkent University, 06800 Ankara, Turkey
*Corresponding author: gurkan.figen@tubitak.gov.tr

Received 10 December 2015; revised 5 February 2016; accepted 22 February 2016; posted 22 February 2016 (Doc. ID 255469); published 18 March 2016

In this paper, we design aperiodic gratings based on orientation-patterned gallium arsenide (OP-GaAs) for converting 2.1 μm pump laser radiation into long-wave infrared (8–12 μm) in an idler-efficiency-enhanced scheme. These single OP-GaAs gratings placed in an optical parametric oscillator (OPO) or an optical parametric generator (OPG) can simultaneously phase match two optical parametric amplification (OPA) processes, OPA 1 and OPA 2. We use two design methods that allow simultaneous phase matching of two arbitrary $\chi^{(2)}$ processes and also free adjustment of their relative strength. The first aperiodic grating design method (Method 1) relies on generating a grating structure that has domain walls located at the zeros of the summation of two cosine functions, each of which has a spatial frequency that equals one of the phase-mismatch terms of the two processes. Some of the domain walls are discarded considering the minimum domain length that is achievable in the production process. In this paper, we propose a second design method (Method 2) that relies on discretizing the crystal length with sample lengths that are much smaller than the minimum domain length and testing each sample's contribution in such a way that the sign of the nonlinearity maximizes the magnitude sum of the real and imaginary parts of the Fourier transform of the grating function at the relevant phase mismatches. Method 2 produces a similar performance as Method 1 in terms of the maximization of the height of either Fourier peak located at the relevant phase mismatch while allowing an adjustable relative height for the two peaks. To our knowledge, this is the first time that aperiodic OP-GaAs gratings have been proposed for efficient long-wave infrared beam generation based on simultaneous phase matching.

OCIS codes: (190.0190) Nonlinear optics; (190.4975) Parametric processes; (190.4970) Parametric oscillators and amplifiers; (140.3070) Infrared and far-infrared lasers.

http://dx.doi.org/10.1364/AO.55.002404

1. INTRODUCTION

Laser sources that can generate long-wave infrared (8–12 μm) beams have important applications in fields such as infrared laser projector technologies, remote sensing, and spectroscopy. CO_2 lasers have been commonly used in such applications; however, solid-state lasers are usually the preferred alternatives due to their compact size and ease of operation.

The gallium arsenide (GaAs) crystal has a large second-order nonlinearity ($d_{14} \sim 94$ pm/V) [1], a wide transparency range (0.9–17 μm), and favorable thermal and mechanical properties. Although birefringent phase matching is not possible due to optical isotropy of the crystal, it is possible to employ quasi-phase matching (QPM) in orientation-patterned GaAs (OP-GaAs) formed by periodic inversions of the crystallographic orientation grown into the crystal [2,3], commonly using hybrid vapor phase epitaxy (HVPE) growing techniques [4–6]. In recent years, this crystal has been employed in optical parametric oscillators (OPOs) [7–13] and seeded OPGs [14] for efficient frequency conversion of laser radiation into the 2–5 μm [7–11,13] and 8–12 μm [7,8,12–14] regions of the spectrum.

The achievable power conversion efficiencies for the conversion of the well-established 2 μm laser sources, such as a Tm:fiber laser pumped Ho:YAG laser, a Tm,Ho:fiber laser, or a Tm,Ho:YLF laser, into the relatively long wavelength region of 8–12 μm are rather low due to the relatively small quantum efficiencies (25%–17% corresponding to the conversion of a 2 μm pump to an 8 μm idler and a 2 μm pump to a 12 μm idler, respectively). One solution is the use of cascaded optical parametric amplification (OPA) processes for the enhancement

of the conversion efficiency of the idler, whose wavelength is in the 8–12 μm band in our case, compared to what is achievable by a single OPA process [15–29]. In such a device, when pumped by a laser source, the signal is amplified, and the idler is generated as a result of the first OPA process (OPA 1). The signal acts as the pump for the second OPA process (OPA 2) and signal photons are further converted into idler and difference-frequency (DF) photons; hence the idler conversion efficiency is enhanced, which means that the 100% limit for the pump-to-idler photon conversion efficiency of the single OPA process can be exceeded.

In order to achieve higher overall conversion efficiencies, rather than cascading OPA 1 and OPA 2 in separate gratings, it is preferable to employ a single grating in which both processes take place by means of simultaneous phase matching (SMPM) [20–28,30–33]. SMPM increases the effective interaction length dedicated to each nonlinear process. Hence it is usually more advantageous to employ a single grating in which two processes are simultaneously phase matched rather than two separate gratings, with a total length equal to that of the single grating, where in each grating only a single process is phase matched. Furthermore, in an idler-efficiency-enhanced device employing SMPM, it is highly desirable to adjust the relative strength of the processes involved to an optimum value by means of the grating design method so that the output conversion efficiency or power is maximized. In [27,28], the design of aperiodically poled MgO-doped $LiNbO_3$ (APMgLN) gratings for an idler-efficiency-enhanced mid-wave infrared (3.8 μm) beam generating seeded OPG were reported. The design with the optimum relative strength of OPA 1 and OPA 2 processes was determined at a given pump power for maximum output efficiency or power.

In this paper, we compare the theoretical performance of two design methods that allow SMPM of two arbitrary $\chi(2)$ processes and also free adjustment of their relative strength. The crystal of these one-dimensional aperiodic gratings is chosen to be OP-GaAs. These single gratings placed in an OPO or an optical parametric generator (OPG) can simultaneously phase match both OPA 1 and OPA 2 for converting the 2.1 μm pump laser radiation into 8–12 μm in an idler-efficiency-enhanced scheme. Recently, a model and its results were reported for an idler-efficiency-enhanced OPO based on two separate OP-GaAs gratings placed in the same cavity for converting 2.1 μm laser radiation into 8–12 μm [29]. However, to our knowledge, single OP-GaAs gratings employing SMPM that are constructed for the same purpose were not proposed before.

The first aperiodic grating design method (Method 1), which was reported in [31], relies on generating an aperiodic grating structure that has domain walls located at the zeros of the summation of two cosine functions, each of which has a spatial frequency that equals one of the phase mismatches of the two processes. In this method some of the domain walls are discarded considering the minimum domain length ($D_{\min}$) that is achievable in the production process. In [27,28], this method was used for designing aperiodic gratings for an idler-efficiency-enhanced mid-wave infrared beam generating seeded OPG.

The second design method (Method 2) relies on discretizing the crystal length with samples of length D_s that are much smaller than $D_{\min}$ and testing each sample's contribution in such a way that the sign of the nonlinearity maximizes the magnitude sum of the real and imaginary parts of the Fourier transform of the grating function at the relevant phase mismatches. Also, during the procedure, the smallest domain length is imposed to be $D_{\min}$. This method has a similar philosophy with the design method presented in [32] that is used for second-harmonic generation at multiple wavelengths. However, our method has a different formulation. It is more general in terms of the selection of the signs of the nonlinearity of each sample, and it has the capability of the adjustment of the relative strength of the Fourier peaks located at the relevant phase mismatches during the grating construction. Also we believe our method yields larger Fourier peak heights and less noise in the Fourier spectrum due to the fact that we use a much smaller length D_s for the sampling, rather than $D_{\min}$.

It was shown that a grating function that is generated using Method 1 is best aligned with a design target in terms of the dot product in Fourier space [33]. In this paper, we propose Method 2, which we find produces a similar performance as Method 1 in terms of the maximization of either Fourier peak height while adjusting the relative height of these peaks. Furthermore, to our knowledge, this is the first time that aperiodic OP-GaAs gratings are proposed for efficient long-wave infrared beam generation based on simultaneous phase matching.

2. APERIODIC GRATINGS FOR LONG-WAVE INFRARED GENERATION

We explain the proposed device structure for long-wave infrared generation and the aperiodic grating design methods applied to the OP-GaAs crystal employed in this device. We compare their performance.

A. Device Structure

The proposed long-wave infrared generating idler-efficiency-enhanced OPO (IEE-OPO) is assumed to be pumped by a 2090 nm laser source that produces nanosecond pulses. The wavelength of the long-wave infrared output of IEE-OPO is chosen to be 10.5 μm. Figure 1 shows the diagram for the device structure of the OPO. The pump beam is focused at the center of an OP-GaAs crystal with a lens L1. We assume that two OPA processes (OPA 1 and OPA 2) are simultaneously phase matched in this single OP-GaAs grating with a length of 50 mm. Mirrors M1 and M2 are highly reflecting at the signal wavelength whereas they are highly transmitting at the pump wavelength $\lambda_p = 2090$ nm. M2 is highly transmitting at the idler and DF wavelength. The cavity is therefore singly resonant. The signal, idler, and DF wavelengths are $\lambda_s = 2609$ nm, $\lambda_i = 10.5$ μm, and $\lambda_{DF} = 3472$ nm, respectively. A seeded OPG without a cavity could also be used for the same purpose, provided that a 2609 nm diode laser is used as an injection seed.

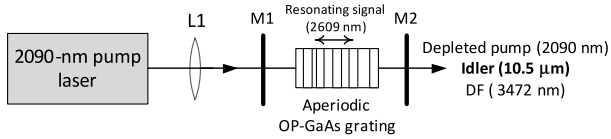

Fig. 1. Diagram of the proposed 10.5 μm generating IEE-OPO.

The IEE-OPO can employ one of the collinear phase-matching geometries given in [9]. In order to maximize the output idler conversion efficiency, it would be beneficial to set all waves linearly polarized along the [111] axis of OP-GaAs so that the value of the nonlinear coefficient (without Miller scaling [34]) for both OPA 1 and OPA 2 is $\sim 1.15 d_{14}$ [9]. The crystal is assumed to be placed in an oven that is kept at a temperature of $T = 40°C$.

B. Grating Design Methods

We employed two grating design methods for constructing the aperiodic OP-GaAs gratings to be used in the IEE-OPO. Both design methods can produce peaks for the magnitude of the Fourier transform of their grating functions with these peaks located at the two phase mismatches of OPA 1 and OPA 2; hence they facilitate SMPM of these processes. With these methods, either one of these Fourier peak heights can be made to be quite large. Furthermore, it is possible to adjust the relative height of these two peaks; hence the relative strength of the processes can be adjusted. It was recently shown that the maximum output efficiency or power can be achieved by optimizing the relative strength of OPA 1 and OPA 2 processes in an idler-efficiency-enhanced seeded OPG [27,28].

1. Method 1

Method 1 starts with the summation of two cosine functions, each of which has a spatial frequency that corresponds to the phase-mismatch term of one of the OPA processes [27,31]; hence

$$f(z) = \cos(\Delta k_{\mathrm{OPA1}} z) + A \cos(\Delta k_{\mathrm{OPA2}} z), \tag{1}$$

where z represents the distance in the propagation direction and A is a parameter whose value is to be adjusted. For each value of A, one obtains a single grating function $g(z)$ that represents the sign of the nonlinearity at each domain and a single value for the relative strength of the two processes.

Here, the phase-mismatch terms corresponding to the two processes are given by

$$\Delta k_{\mathrm{OPA1}} = k_p - k_s - k_i, \tag{2}$$

$$\Delta k_{\mathrm{OPA2}} = k_s - k_i - k_{\mathrm{DF}}, \tag{3}$$

with k_p, k_s, k_i, and k_{DF} being the wavenumbers of the pump, signal, idler, and difference frequency, respectively. The phase-mismatch terms at the chosen wavelengths and at $T = 40°C$ are $\Delta k_{\mathrm{OPA1}} = 7.4867 \times 10^4\ \mathrm{m}^{-1}$ and $\Delta k_{\mathrm{OPA2}} = 5.1295 \times 10^4\ \mathrm{m}^{-1}$. These are calculated using the refractive index equation given in [35] for GaAs.

The zero crossings of the function given in Eq. (1) yield the domain wall locations of the OP-GaAs, and hence the grating function is given as

$$g(z) = \mathrm{sgn}[f(z)], \tag{4}$$

where sgn represents the signum function.

Next, the restriction of achievable minimum domain length (D_{min}) is imposed, which is a restriction of the production process. We use $D_{\mathrm{min}} = 16\ \mu\mathrm{m}$, which is a feasible value in current HVPE growth technology. We sequentially flip the sign of the shortest domain of $g(z)$ whose length is less than D_{min} until there are no domains left shorter than this length. At the end of this step, we also round off the domain wall locations to the nearest 1 μm increment considering the feasible resolution for the photolithographic mask.

The normalized Fourier transform of the resulting grating function $g(z)$ is given as

$$G(\Delta k) = \frac{1}{l_c} \int_0^{l_c} g(z) \exp(-j \Delta k z) \mathrm{d}z, \tag{5}$$

where l_c is the grating length.

The Fourier-domain function $|G(\Delta k)|$ has peaks at Δk_{OPA1} and Δk_{OPA2}, which facilitate the SMPM of these interactions. We define

$$\alpha = \frac{|G(\Delta k_{\mathrm{OPA2}})|}{|G(\Delta k_{\mathrm{OPA1}})|}, \tag{6}$$

which yields the magnitude ratio of these peak heights.

The effective nonlinear coefficients for the two OPA processes are given by

$$d_e^{\mathrm{OPA1}} \simeq 1.15 |G(\Delta k_{\mathrm{OPA1}}) d_{14}^{\mathrm{OPA1}}|, \tag{7}$$

$$d_e^{\mathrm{OPA2}} \simeq 1.15 |G(\Delta k_{\mathrm{OPA2}}) d_{14}^{\mathrm{OPA2}}|, \tag{8}$$

when all waves are polarized along the [111] axis of OP-GaAs [9]. Also, $d_{14} \sim 94$ pm/V for the second-harmonic generation of 4.1 μm in OP-GaAs [1]; d_{14}^{OPA1} and d_{14}^{OPA2} are obtained by scaling d_{14} with Miller's rule [34] for OPA 1 and OPA 2, respectively. Hence, the relative strength of the two OPA processes is given by

$$\frac{d_e^{\mathrm{OPA2}}}{d_e^{\mathrm{OPA1}}} = \left| \frac{d_{14}^{\mathrm{OPA2}}}{d_{14}^{\mathrm{OPA1}}} \right| \alpha \simeq 0.98 \alpha. \tag{9}$$

2. Method 2

In Method 2, the crystal length is discretized with samples of length D_s, and each sample's contribution is tested in such a way that the sign of the nonlinearity maximizes the magnitude sum of the real and imaginary parts of the Fourier transform of the grating function at the relevant phase-mismatch terms. As in Method 1, the shortest domain length is chosen to be $D_{\mathrm{min}} = 16\ \mu\mathrm{m}$ due to the restriction of production process, and a much smaller value, 1 μm, is used for D_s.

The normalized Fourier transform of the grating function $g(z)$ given in Eq. (5) can be approximated as follows:

$$G(\Delta k) \approx \frac{1}{l_c} \sum_{n=1}^{N} [g(D_s n) \cos(\Delta k D_s n) - j g(D_s n) \sin(\Delta k D_s n)], \tag{10}$$

where N is the number of samples with $N D_s = l_c$ ($N = 50,000$ for $l_c = 50$ mm) and $g(D_s n) = (-1)^m$ with $m = 1$ or 2 for $n = 1, \ldots, N$. Depending on the sign of the nonlinearity dictated by the grating function $g(D_s n)$, m is either 1 or 2 at each sample with index n.

One observes that there are two contributions to the summation that yield the Fourier transform at a given Δk from each sample with index n: The first one is a real term $[(-1)^m \cos(\Delta k D_s n)/l_c]$, and the second one is an imaginary term $[-(-1)^m j \sin(\Delta k D_s n)/l_c]$.

Consequently, starting at $n = 1$ and ending at $n = N$, we can construct a grating function by choosing the sign of the

nonlinearity at each sample. This is possible by selecting the sign of the nonlinearity at each sample such that the sum of the magnitudes of the real and imaginary parts of the Fourier transform at Δk_{OPA1} and Δk_{OPA2} is maximized with a certain weight that will either favor the term calculated at Δk_{OPA1} or the one at Δk_{OPA2}. For this purpose, we define the following test function and apply the following selection procedure:

$$\begin{aligned} f_{\mathrm{test}}(D_s n) \triangleq\ & s_1(-1)^m \cos(\Delta k_{\mathrm{OPA1}} D_s n) \\ & + s_2(-1)^m \sin(\Delta k_{\mathrm{OPA1}} D_s n) \\ & + A s_3(-1)^m \cos(\Delta k_{\mathrm{OPA2}} D_s n) \\ & + A s_4(-1)^m \sin(\Delta k_{\mathrm{OPA2}} D_s n), \end{aligned} \tag{11}$$

where A is the weight parameter, which is also used for adjusting the relative strength of the two processes and $s_i = +1$ or -1 (for $i = 1, 2, 3,$ or 4).

For each of the eight cases corresponding to $(s_1\ s_2\ s_3\ s_4) = (+1-1-1-1), (+1-1-1+1), \ldots, (+1+1+1+1)$, where s_1 is chosen to be $+1$, we calculate f_{test} at each sample from $n = 1$ to N, and we choose either $m = 1$ or $m = 2$, whichever gives the largest value of f_{test}. We obtain eight grating functions at the end. Here, since the magnitude of each term on the right-hand side of Eq. (11) does not change depending on the sign in front of the term, there are eight cases, each of which yields the same value for the magnitude of each term.

For efficient operation, it is desirable to have the grating energy concentrated at the Fourier peak locations, Δk_{OPA1} and Δk_{OPA2}. Hence, we select the grating function that yields the largest normalized grating energy (NGE) [27] given by

$$\mathrm{NGE} = (|G(\Delta k_{\mathrm{OPA1}})|^2 + |G(\Delta k_{\mathrm{OPA2}})|^2)/(2/\pi)^2. \tag{12}$$

We note that $2/\pi$ is the largest Fourier coefficient that can be obtained for a periodic grating, which is attainable if the grating has a 50% duty cycle [36]. However, we should also note that for the given l_c, D_s, $D_{\min}$, Δk_{OPA1}, and Δk_{OPA2} values, the resultant NGE values (in percent) are approximately the same within 2 percentage points for all eight gratings. We will also use NGE for comparing the performance of Method 2 with that of Method 1.

Last, we employ Eqs. (6), (9), and (10) for calculating the relative strength of the two processes.

C. RESULTS AND DISCUSSION

We first present the aperiodic grating structures obtained using Method 1 and Method 2 for various values of α along with the dependence of α on coefficient A that is used for generating these gratings.

We discuss the spectral and temperature phase-matching bandwidths of the gratings and the amount of temperature tuning necessary if the pump laser wavelength does not match with the design wavelength. Last, we discuss the systematic error in domain wall locations that occurs in OP-GaAs gratings during the growth process and the effects of this error on grating performance.

1. Grating Structures

We have chosen $0 \le \alpha \le 2$ as the region of interest [27,28] for designing our aperiodic gratings based on OP-GaAs. When $\alpha = 0$, the grating is periodic, OPA 2 does not take place, and there is no idler-efficiency enhancement. When $\alpha = 2$, the effective nonlinearity of OPA 2 is approximately twice that of OPA 1; hence as the signal is strongly converted into idler and DF, the resonant signal experiences a relatively large nonlinear loss, which means that the IEE-OPO will be below threshold for ordinary pumping levels. Consequently, within this α range, one would expect to have the optimum α where the idler-efficiency enhancement is at its maximum.

In Fig. 2(a), the α values that are obtained at the end of the procedure of Method 1 and Method 2 are plotted against different values of the coefficient A given in Eqs. (1) and (11), respectively. It can be seen that for $A \le 0.9$, the α values obtained with both methods are approximately the same. Figure 2(b) shows NGE values that are obtained with both methods for the same range of α values. With Method 2, as in Method 1, it is possible to have the grating energy highly concentrated at the Fourier peak locations, Δk_{OPA1} and Δk_{OPA2}. The NGE values that are obtained with Method 2 are slightly better. For both methods, it can be seen that the NGE dedicated to the two OPA processes has a minimum value of 81% at around $\alpha = 1.0$; hence 19% of the NGE is not usable in SMPM. We note here that this unusable portion of NGE is due to the Fourier peaks (of $|G(\Delta k)|$) that occur at locations other than Δk_{OPA1} and Δk_{OPA2}. Such peaks are shown in Fig. 6 given at the end of this section.

We define the *optimized* function F_{opt} as follows:

$$\begin{aligned} F_{\mathrm{opt}} \triangleq\ & |\mathrm{Re}\{G(\Delta k_{\mathrm{OPA1}})\}| + |\mathrm{Im}\{G(\Delta k_{\mathrm{OPA1}})\}| \\ & + A[|\mathrm{Re}\{G(\Delta k_{\mathrm{OPA2}})\}| + |\mathrm{Im}\{G(\Delta k_{\mathrm{OPA2}})\}|], \end{aligned} \tag{13}$$

where functions Re and Im give the real and imaginary parts of their arguments, respectively. In Fig. 3, we plot F_{opt} as a function of the resultant α for both methods. Although NGE values for the two methods are almost equal, F_{opt} values are quite different from each other.

Equations (11) and (13) are closely related. Equation (11) is used for selecting the sign of the nonlinearity at each sample that maximizes the sum of the magnitudes of the real (cos terms) and imaginary (sin terms) parts of the Fourier transform contributions calculated at Δk_{OPA1} and Δk_{OPA2} (except the scaling with $1/l_c$), where also a weight coefficient A is used. Similarly, Eq. (13) does the same calculation for the whole grating structure. (The scaling with $1/l_c$ is included in this case.) In fact, F_{opt} is the collection of the magnitude of Fourier transform contributions that are maximized in Method 2 during

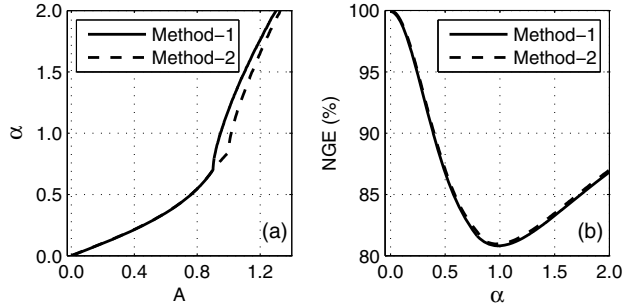

Fig. 2. (a) Plot of α as a function of coefficient A. (b) Plot of NGE (in percent) as a function of α.

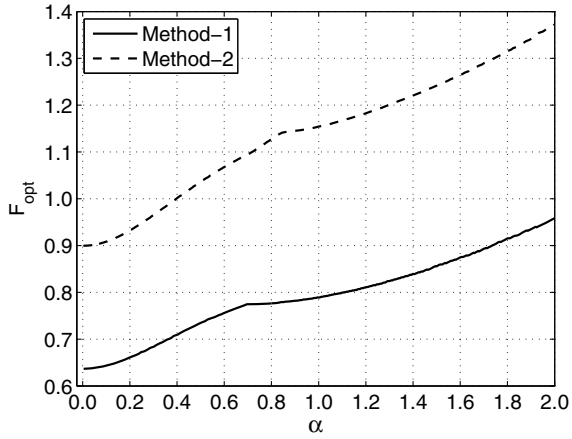

Fig. 3. Plot F_{opt} given in Eq. (13) as a function of α for both methods.

the construction of the whole grating. Therefore, Method 2 produces the optimum values for F_{opt} as shown in Fig. 3.

However, from Fig. 3, one observes that optimum values are not obtained if F_{opt} is calculated using the gratings designed by Method 1. This is an indication that the two methods produce different grating structures. We should note that when calculating Eq. (13) for each method, we used the values of the A coefficient for the particular method. Also, as seen from Fig. 2(a), the values of the A coefficient for the two methods are similar. Hence it is still possible to make a fair comparison of the F_{opt} function calculated by the two methods. We conclude that considering their F_{opt} values, Method 1 and Method 2 produce different grating structures, but considering their NGE values, these gratings will yield similar idler output efficiencies for the IEE-OPO.

In Fig. 4, we provide the plots showing the lengths of inverted and noninverted domains as functions of domain order for three gratings with $\alpha = 0.3$, $\alpha = 0.7$, and $\alpha = 1.5$ ($l_c = 50$ mm), which were generated using Method 1. In Fig. 5, we provide similar plots for the same α values while the gratings were generated using Method 2.

Consider the gratings generated using Method 1: For the grating with $\alpha = 0.3$, there are 1192 domains. Both inverted and noninverted domains have varying lengths between 32 μm and 48 μm. For the grating with $\alpha = 0.7$, there are 1193 domains. Both inverted and noninverted domains have varying lengths between 16 μm and 50 μm. For the grating with $\alpha = 1.5$, there are only 875 domains. Both inverted and noninverted domains have varying lengths that are mainly centered at around 22 μm, 51 μm, and 97 μm. Considering the gratings generated using Method 2, similar distributions for the lengths of inverted and noninverted domains are obtained. However, a closer look will reveal the differences in domain lengths compared to those produced by Method 1.

Plots of the magnitude of the normalized Fourier transform ($|G(\Delta k|$) of the gratings that were generated using Method 2 are shown in Fig. 6. The peaks that are used for the SMPM of the two OPA processes are marked in each plot. As is typical with all grating structures, in each plot there are some unused peaks that result in a decrease in the effective nonlinearities of the processes. The plots for the gratings generated using Method 1 are similar but not shown.

In Method 2, we use two different feature lengths, D_s and D_{min}, where D_s is much smaller than D_{min}. This enables us to have domains with lengths $D_{\text{min}} \le l_d \le 2D_{\text{min}}$, $2D_{\text{min}} \le l_d \le 3D_{\text{min}}$, etc. However, as an extreme case, if we set $D_s = D_{\text{min}}$, we would only have domains with lengths D_{min}, $2D_{\text{min}}$, etc. In this case, for a given α value, both $|G(\Delta k_{\text{OPA1}})|$

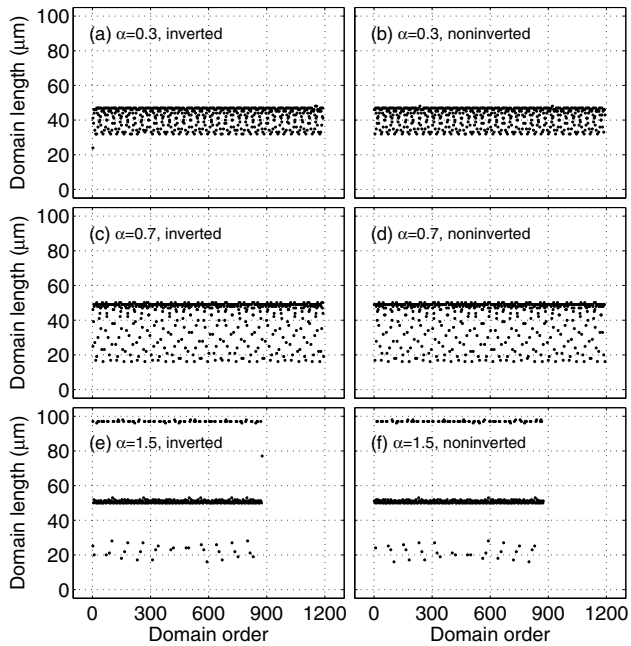

Fig. 4. Lengths of the inverted and noninverted domains of the gratings with $\alpha = 0.3$, $\alpha = 0.7$, and $\alpha = 1.5$ as functions of domain order ($l_c = 50$ mm). Gratings were generated using Method 1.

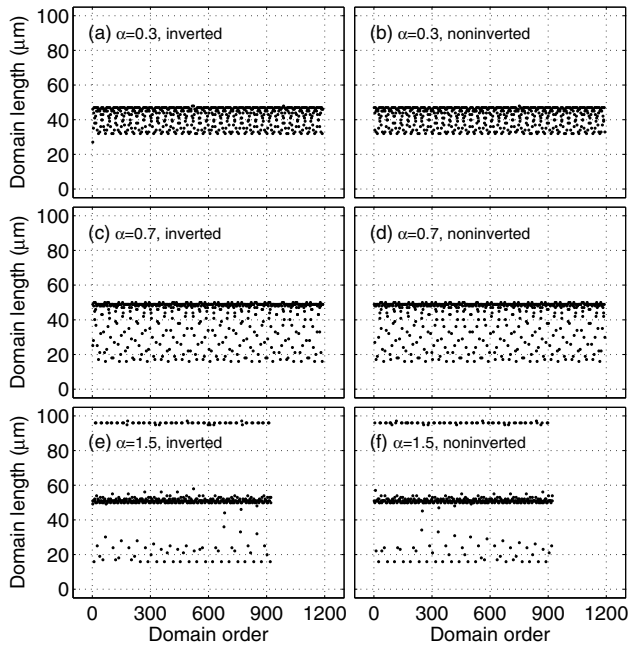

Fig. 5. Lengths of the inverted and noninverted domains of the gratings with $\alpha = 0.3$, $\alpha = 0.7$, and $\alpha = 1.5$ as functions of domain order ($l_c = 50$ mm). Gratings were generated using Method 2.

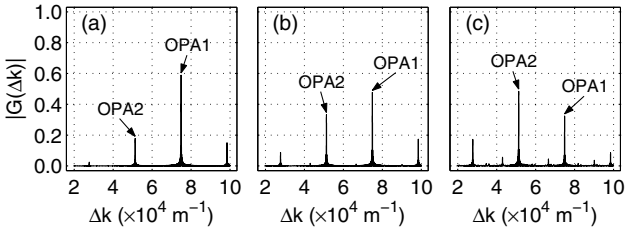

Fig. 6. Magnitudes of the normalized Fourier transforms ($|G(\Delta k)|$) of the gratings with (a) $\alpha = 0.3$, (b) $\alpha = 0.7$, and (c) $\alpha = 1.5$. For all gratings, $l_c = 50$ mm. The gratings were generated using Method 2. The peaks that are used for the SMPM of OPA 1 and OPA 2 are marked in each plot.

and $|G(\Delta k_{\mathrm{OPA2}})|$ values would be lower compared to the case in which D_s is much smaller than $D_{\min}$. For instance, at $\alpha = 0.3$, when $D_s = D_{\min} = 16$ μm, both $|G(\Delta k_{\mathrm{OPA1}})|$ and $|G(\Delta k_{\mathrm{OPA2}})|$ are lower by 5.5% than what they would be when $D_s = 1$ μm and $D_{\min} = 16$ μm. Also NGE is lower with ∼10 percentage points, and there will be more noise in the Fourier spectrum ($|G(\Delta k|$). The overall result will be a significant decrease in output conversion efficiency. Consequently, in Method 2, it is necessary to use a much smaller D_s compared to $D_{\min}$.

Both Method 1 and Method 2 are fast algorithms. It typically takes about four times shorter with Method 1 to calculate one grating structure for a given A coefficient.

2. Phase-Matching Bandwidths and Tolerances

We first determined the spectral and temperature phase-matching bandwidths for the IEE-OPO based on the aperiodic OP-GaAs gratings. For this calculation, we needed to determine the distance between the locations of the first two zeros of $|G(\Delta k)|$ (in Δk domain) around each Fourier peak corresponding to OPA 1 or OPA 2. Our analysis is similar to what is given in [27].

Regardless of the design method employed, the grating function can be described as a multiplication of a step function that is zero for $z < 0$ or $z > l_c$ and 1 for $0 \le z \le l_c$ with another function that has the grating structure for $0 \le z \le l_c$. The multiplication corresponds to convolution operation in Fourier space; hence both Fourier peaks have the characteristics of a *sinc* function, which is the Fourier transform of the step function. The first two zeros around each of the peaks are separated by a distance of $4\pi/l_c$, provided that the longest domain length in the grating is much shorter than l_c, a condition that is always satisfied. These zero locations around each peak mark the passband of a process. We note that $4\pi/l_c = 251.3$ m^{-1} for $l_c = 50$ mm.

We use the passband definition given above rather than the full-width-half-maximum (FWHM) definition that is usually employed for determining the phase-matching bandwidths. The reason for this is that the idler power conversion efficiency may not have the characteristics of a sinc^2 function for the dependence on $\Delta k l_c/2$, which happens to be the case when there is a single process involved, the undepleted pump approximation is valid, and all waves are assumed to be plane waves [37]. However, none of these conditions or assumptions are generally valid for the IEE-OPO. One must note that the phase-matching bandwidth determined using our definition above usually represents an upper limit and the bandwidth over which there is significant idler output will be lower.

We determined the pump wavelength (λ_p) that can be phase matched when both phase mismatches are located either at the lower or the higher limits of the passband of OPA 1 and OPA 2 processes. We summed up the absolute values of the shifts in λ_p (±2.3 nm) that are required to satisfy the phase matching condition for these two cases. Consequently, the spectral phase-matching bandwidth (defined as from-zero-to-zero, not as a FWHM) for the pump is 4.6 nm for the OP-GaAs gratings with $l_c = 50$ mm (regardless of the design method employed and the value of α). As the grating length becomes shorter, the bandwidth becomes larger in accordance with the $4\pi/l_c$ expression for the passband above. We kept the operating temperature of the crystal fixed at $T = 40$°C and used numerical root-finding techniques to calculate this result. It is also noted that when λ_p increases by 2.3 nm, λ_s and λ_{DF} increase by 4.1 nm and 8.4 nm, respectively, whereas λ_i decreases by 10.1 nm.

We note here that if we assume that OPA 1 phase mismatch is located at the lower (or higher) limit of the passband while OPA 2 phase mismatch is located at the higher (or lower) limit of the passband, respectively, we obtain shifts in λ_p that are about ±0.7 nm for these two cases and a total of 1.4 nm spectral bandwidth. Hence the 4.6 nm value represents the largest possible spectral bandwidth for the pump that can be obtained using this calculation.

We performed a similar calculation for estimating the temperature phase-matching bandwidth of the IEE-OPO. We determined the temperature (T) for satisfying phase matching while λ_p is kept fixed at 2090 nm and when both phase mismatches are located either at the lower or the higher limits of the passband of OPA 1 and OPA 2 processes. We summed up the absolute values of the shifts in T (±6.6°C) that are required to satisfy the phase matching condition for these two cases. Consequently, the temperature phase-matching bandwidth turns out to be 13.2°C for the IEE-OPO based on OP-GaAs gratings with $l_c = 50$ mm (regardless of the design method employed and the value of α). It is also noted that when T increases by 6.6°C, λ_s and λ_{DF} decrease by 1.2 nm and 4.4 nm, respectively, whereas λ_i increases by 21.1 nm.

Next, we calculate the amount of the temperature tuning for the IEE-OPO that would be needed if the pump wavelength differs from the design wavelength, 2090 nm. The pump lasers that can be used for the long-wave infrared generating IEE-OPO usually have a fixed value for λ_p. It is important to choose this λ_p to be almost equal to 2090 nm in order to use the gratings presented in this paper for efficient idler generation. Also the linewidth of the pump laser is to be much smaller than 4.6 nm (the spectral phase-matching bandwidth) in order not to have a reduction in output efficiency compared to what would be expected with a single-frequency pump source. However, if λ_p does not coincide with 2090 nm, one can tune the temperature of the OP-GaAs grating in the IEE-OPO so that all other wavelengths (signal, idler, and DF) are tuned and the phase-mismatch values are readjusted to be the design values $\Delta k_{\mathrm{OPA1}} = 7.4867 \times 10^4$ m^{-1} and $\Delta k_{\mathrm{OPA2}} = 5.1295 \times 10^4$ m^{-1}.

Figure 7 shows the operating temperature restoring the phase matching as a function of the pump wavelength for

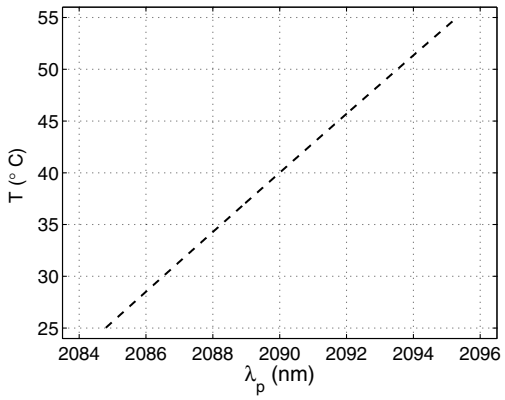

Fig. 7. Operating temperature restoring the phase matching as a function of λ_p for the grating with $\alpha = 0.3$ that was originally designed for $\lambda_p = 2090$ nm and $T = 40$°C. The grating was generated using Method 1.

the grating that was originally designed for $\lambda_p = 2090$ nm and $T = 40$°C. For instance, from the figure, one observes that if λ_p happens to be 2092 nm, one needs to set $T = 45.7$°C to have efficient conversion into the idler wavelength. We also note that when $\lambda_p = 2085$ nm ($\lambda_p = 2095$ nm), λ_s, λ_i, and λ_{DF} decreases (increases) by 6.6 nm, 18.8 nm, and 9.7 nm. The plot is for the grating with $\alpha = 0.3$ that was designed with Method 1. However, the results are approximately the same regardless of the design method employed or the value of α.

Next, we determined the effect of systematic errors that occur at the positions of the domain boundaries of OP-GaAs gratings during the HVPE growth process. It is noted that there is usually no measurable amount of randomness in the domain wall locations in OP-GaAs gratings; however, there is a systematic change in the positions of the domain walls depending on the depth within the crystal [38]. For example, if the template used during the HVPE growth process were a periodic grating with a duty cycle of 50%, the resulting duty cycle would be 50% at locations near the template and less than 50% at locations further away, whereas the period would remain unchanged. For an aperiodic OP-GaAs grating with an active thickness of about 650 μm, one can expect that the length of the inverted domains to systematically decrease by a few micrometers from the bottom of the crystal to the top of the crystal, whereas the sum of the lengths of an inverted and a noninverted domain that are adjacent to each other remains unchanged. For thicker gratings the systematic error will be larger.

We considered the effect of this systematic error for three values of the amount of reduction in the length of the inverted domains, $\Delta l = 1$ μm, 3 μm, and 5 μm. The results are approximately the same regardless of the design method employed or the value of α.

We performed the length reduction for all inverted domains in a particular grating, and we kept the sum of the lengths of one inverted and one noninverted domain within a local period unchanged. We observed that for all Δl values, the fractional errors in placing the Fourier peaks at Δk_{OPA1} ($= |\Delta k_{New1} - \Delta k_{OPA1}|/\Delta k_{OPA1}$) and at Δk_{OPA2}($= |\Delta k_{New2} - \Delta k_{OPA2}|/\Delta k_{OPA2}$) are in the order of 10^{-6}, where Δk_{New1} and Δk_{New2} are the locations of the two Fourier peaks of the modified $|G(\Delta k)|$ after the systematic error was implemented on the grating structure. This fractional error corresponds to a wavelength shift in the pump wavelength, which is in the order of 10^{-3} nm, a quite small value compared with the linewidth of the pump laser, which is typically less than 1 nm (FWHM); hence it is negligible.

We observed that the value of NGE decreases with an increasing amount of inverted-domain length reduction. For the grating with $\alpha = 0.3$ generated with Method 1, NGE = 92.9%, 91.9%, and 89.9% for $\Delta l = 1$ μm, 3 μm, and 5 μm, respectively. The result is a slight reduction in output efficiency. Also, the value of α for the systematic-error-implemented grating slightly increases (within ~2%), as Δl increases. Similarly, for the grating with $\alpha = 0.3$ generated with Method 2, NGE = 93.1%, 92.1%, and 90.2% for $\Delta l = 1$ μm, 3 μm, and 5 μm, respectively.

When $\Delta l = 5$ μm, the value of NGE is lower by ~3, ~2, and ~2 percentage points for $\alpha = 0.3$, $\alpha = 0.7$, and $\alpha = 1.5$ gratings, respectively, compared to the case when there is no systematic error in these gratings. When $\Delta l = 5$ μm, we further simulated the effect of a random error at the domain wall locations that might be present due to unidentified effects. For this purpose, we added random numbers to the domain wall locations from a zero-mean uniform distribution with an rms error of $\sigma = 1$ μm. In this case, the fractional error in placing the Fourier peaks at the original locations is slightly higher and the corresponding pump wavelength shift is in the order of 10^{-2} nm, still a quite low value. Also, this random error introduces a further ~0.5 percentage point decrease in the value of NGE. Consequently, errors in the domain wall locations of OP-GaAs gratings that occur due to the artifacts of the current growth technology are expected to only weakly affect the performance of IEE-OPOs.

3. CONCLUSION

In this paper, we proposed aperiodic OP-GaAs gratings that can simultaneously phase match two OPA processes for the conversion of a 2.1 μm laser radiation into 8–12 μm based on an IEE-OPO or an IEE-OPG. We used two design methods for generating these gratings and compared their performance. To our knowledge, this is the first time that aperiodic OP-GaAs gratings are proposed for efficient long-wave infrared beam generation based on single gratings that can perform SMPM.

In this work, we have only concentrated on the grating design methods that can be employed for designing such OP-GaAs gratings. The next step is to determine the optimum α, which maximizes the conversion efficiency or output power of the 8–12 μm output beam. Such an optimization based on a realistic model that takes the diffraction of the beams into account was recently reported for an IEE-OPG employing APMgLN gratings in which the relative strength of OPA 1 and OPA 2 processes was optimized at a given pump power for maximum output efficiency or power [27,28]. We reserve the use of a similar model for the proposed single-grating IEE-OPO for future work.

However, we note here that a similar model for a long-wave infrared IEE-OPO based on two separate OP-GaAs gratings

placed in the same cavity was recently developed [29], and the improvement in the output efficiency due to intracavity idler enhancement was quantified. For the same total crystal length, one would expect to achieve even larger improvement in the output conversion efficiencies if single OP-GaAs gratings similar to what we report in this work are employed for the SMPM of OPA 1 and OPA 2 instead of two separate gratings, that is, one for OPA 1 and one for OPA 2.

We used two methods for designing the aperiodic OP-GaAs gratings. Method 1 relies on generating a grating structure that has domain walls located at the zeros of the summation of two cosine functions, each of which has a spatial frequency that equals one of the phase mismatches of the two processes. We proposed Method 2, which relies on discretizing the crystal length with samples and testing each sample's contribution in such a way that the sign of the nonlinearity maximizes the magnitude sum of the real and imaginary parts of the Fourier transform of the grating function at the relevant phase mismatches. In this work, we compared their performance.

We believe Method 1 and Method 2 will be the methods of choice for designing aperiodic gratings that are employed in idler-efficiency-enhanced parametric devices for infrared beam generation. It was previously shown that a grating function that is generated using Method 1 is best aligned with a design target in terms of the dot product in Fourier space [33]. We have found that Method 2 is also a fast algorithm (similar to Method 1), and it even performs slightly better in terms of the maximization of either Fourier peak height. Both methods facilitate the free adjustment of the relative Fourier peak heights and hence the relative strength of OPA 1 and OPA 2, which is crucial for optimizing the output efficiency or power.

Although the results are not reported in this work, we also implemented two global optimization algorithms, the simulated annealing algorithm [39] and the genetic algorithm [40], for designing aperiodic gratings whose $|G(\Delta k)|'$ s have Fourier peaks located at the phase mismatches with adjustable relative peak heights. We have observed that these algorithms run drastically slower than Method 1 and Method 2, and they are never able to achieve a Fourier peak height (for either one of the peaks) as large as the one obtained by Method 1 or Method 2. We even tried to use one or more grating structures generated by Method 1 as the seed individuals in the population for the genetic algorithm, but we found that the genetic algorithm was not able to converge to a grating structure that performed as good as the initial seed(s).

Funding. TÜBİTAK BİLGEM Research Center, Gebze/Kocaeli, Turkey.

Acknowledgment. Z. G. Figen acknowledges the support provided by the managements of TÜBİTAK BİLGEM Research Center and TÜBİTAK BİLGEM/İLTAREN Research Institute. Z. G. Figen acknowledges fruitful discussions with Dr. Tolga Kartaloğlu of Bilkent University.

REFERENCES

1. T. Skauli, K. L. Vodopyanov, T. J. Pinguet, A. Schober, O. Levi, L. A. Eyres, M. M. Fejer, J. S. Harris, B. Gerard, L. Becouarn, E. Lallier, and G. Arisholm, "Measurement of the nonlinear coefficient of orientation-patterned GaAs and demonstration of highly efficient second-harmonic generation," Opt. Lett. **27**, 628–630 (2002).
2. J. A. Armstrong, N. Bloembergen, J. Ducuing, and P. S. Pershan, "Interactions between light waves in a nonlinear dielectric," Phys. Rev. **127**, 1918–1939 (1962).
3. A. Szilagyi, A. Hordvik, and H. Schlossberg, "A quasi-phase-matching technique for efficient optical mixing and frequency doubling," J. Appl. Phys. **47**, 2025–2032 (1976).
4. L. A. Eyres, P. J. Tourreau, T. J. Pinguet, C. B. Ebert, J. S. Harris, M. M. Fejer, L. Becouarn, B. Gerard, and E. Lallier, "All epitaxial fabrication of thick, orientation-patterned GaAs films for nonlinear optical frequency conversion," Appl. Phys. Lett. **79**, 904–906 (2001).
5. D. F. Bliss, C. Lynch, D. Weyburne, K. O'Hearn, and J. S. Bailey, "Epitaxial growth of thick GaAs on orientation-patterned wafers for nonlinear optical applications," J. Cryst. Growth **287**, 673–678 (2006).
6. R. D. Peterson, D. Whelan, D. Bliss, and C. Lynch, "Improved material quality and OPO performance in orientation-patterned GaAs," Proc. SPIE **7197**, 719709 (2009).
7. K. L. Vodopyanov, O. Levi, P. S. Kuo, T. J. Pinguet, J. S. Harris, M. M. Fejer, B. Gerard, L. Becouarn, and E. Lallier, "Optical parametric oscillation in quasi-phase-matched GaAs," Opt. Lett. **29**, 1912–1914 (2004).
8. K. L. Vodopyanov, O. Levi, P. S. Kuo, T. J. Pinguet, J. S. Harris, M. M. Fejer, B. Gerard, L. Becouarn, and E. Lallier, "Optical parametric oscillator based on microstructured GaAs," Proc. SPIE **5620**, 63–69 (2004).
9. P. S. Kuo, K. L. Vodopyanov, M. M. Fejer, X. Yu, J. S. Harris, D. F. Bliss, and D. Weyburne, "GaAs optical parametric oscillator with circularly polarized and depolarized pump," Opt. Lett. **32**, 2735–2737 (2007).
10. C. Kieleck, M. Eichhorn, A. Hirth, D. Faye, and E. Lallier, "High-efficiency 20–50 kHz mid-infrared orientation-patterned GaAs optical parametric oscillator pumped by a 2 μm holmium laser," Opt. Lett. **34**, 262–264 (2009).
11. C. Kieleck, A. Hildenbrand, M. Eichhorn, D. Faye, E. Lallier, B. Gérard, and S. D. Jackson, "OP-GaAs OPO pumped by 2 μm Q-switched lasers: Tm;Ho:silica fiber laser and Ho:YAG laser," Proc. SPIE **7836**, 783607 (2010).
12. R. K. Feaver, R. D. Peterson, and P. E. Powers, "Longwave-IR optical parametric oscillator in orientation-patterned GaAs pumped by a 2 μm Tm, Ho:YLF laser," Opt. Express **21**, 16104–16110 (2013).
13. K. L. Vodopyanov, I. Makasyuk, and P. G. Schunemann, "Grating tunable 4–14 μm GaAs optical parametric oscillator pumped at 3 μm," Opt. Express **22**, 4131–4136 (2014).
14. O. Levi, T. J. Pinguet, T. Skauli, L. A. Eyres, K. R. Parameswaran, J. S. Harris, Jr., M. M. Fejer, T. J. Kulp, S. E. Bisson, B. Gerard, E. Lallier, and L. Becouarn, "Difference frequency generation of 8-μm radiation in orientation-patterned GaAs," Opt. Lett. **27**, 2091–2093 (2002).
15. M. E. Dearborn, K. Koch, G. T. Moore, and J. C. Diels, "Greater-than 100% photon-conversion efficiency from an optical parametric oscillator with intracavity difference-frequency mixing," Opt. Lett. **23**, 759–761 (1998).
16. K. A. Tillman, D. T. Reid, D. Artigas, and T. Y. Jiang, "Idler-resonant femtosecond tandem optical parametric oscillator tuning from 2.1 μm to 4.2 μm," J. Opt. Soc. Am. B **21**, 1551–1558 (2004).
17. W. Zhang, "High idler conversion with an intracavity optical parametric oscillator and difference frequency generation," Opt. Commun. **274**, 451–455 (2007).
18. J. W. Haus, A. Pandey, and P. E. Powers, "Boosting quantum efficiency using multi-stage parametric amplification," Opt. Commun. **269**, 378–384 (2007).
19. J. M. Fraser and C. Ventalon, "Parametric cascade downconverter for intense ultrafast mid-infrared generation beyond the Manley-Rowe limit," Appl. Opt. **45**, 4109–4113 (2006).
20. H. C. Guo, Y. Q. Qin, Z. X. Shen, and S. H. Tang, "Mid-infrared radiation in an aperiodically poled $LiNbO_3$ superlattice induced by cascaded parametric processes," J. Phys. **16**, 8465–8474 (2004).
21. G. Porat, O. Gayer, and A. Arie, "Simultaneous parametric oscillation and signal-to-idler conversion for efficient downconversion," Opt. Lett. **35**, 1401–1403 (2010).

22. X. Wei, Y. Peng, W. Wang, X. Chen, and D. Li, "High-efficiency mid-infrared laser from synchronous optical parametric oscillation and amplification based on a single MgO:PPLN crystal," Appl. Phys. B **104**, 597–601 (2011).
23. T. Chen, B. Wu, W. Liu, P. Jiang, J. Kong, and Y. Shen, "Efficient parametric conversion from 1.06 to 3.8 μm by an aperiodically poled cascaded lithium niobate," Opt. Lett. **36**, 921–923 (2011).
24. Y. H. Liu, X. J. Lv, Z. D. Xie, X. P. Hu, Y. Yuan, J. Lu, L. N. Zhao, G. Zhao, and S. N. Zhu, "Amplification assisted optical parametric oscillator in the mid-infrared region," Appl. Phys. B **106**, 267–270 (2012).
25. O. P. Naraniya, M. R. Shenoy, and K. Thyagarajan, "Multiple-wavelength quasi-phase-matching for efficient idler generation in $MgO:LiNbO_3$ based nanosecond optical parametric oscillator," Appl. Opt. **51**, 1312–1317 (2012).
26. T. Chen, B. Wu, P. Jiang, D. Yang, and Y. Shen, "High power efficient 3.81 μm emission from a fiber laser pumped aperiodically poled cascaded lithium niobate," IEEE Photon. Tech. Lett. **25**, 2000–2002 (2013).
27. Z. G. Figen, "Seeded optical parametric generator with efficiency-enhanced mid-wave infrared beam output," J. Mod. Opt. **61**, 1269–1281 (2014).
28. Z. G. Figen, "Efficiency-enhanced mid-wave infrared beam generation at 3.8 μm with a seeded optical parametric generator," Proc. SPIE **9251**, 92510E (2014).
29. R. K. Feaver, R. D. Peterson, J. W. Haus, and P. E. Powers, "Cascaded OPGaAs OPO for increased longwave efficiency," Proc. SPIE **9347**, 93470P (2015).
30. R. A. Andrews, H. Rabin, and C. L. Tang, "Coupled parametric down-conversion and upconversion with simultaneous phase matching," Phys. Rev. Lett. **25**, 605–608 (1970).
31. T. Kartaloğlu, Z. G. Figen, and O. Aytür, "Simultaneous phase matching of optical parametric oscillation and second-harmonic generation in aperiodically poled lithium niobate," J. Opt. Soc. Am. B **20**, 343–350 (2003).
32. M. Lu, X. Chen, Y. Chen, and Y. Xia, "Algorithm to design aperiodic optical superlattice for multiple quasi-phase matching," Appl. Opt. **46**, 4138–4143 (2007).
33. A. H. Norton and C. M. de Sterke, "Aperiodic 1-dimensional structures for quasi-phase matching," Opt. Express **12**, 841–846 (2004).
34. D. A. Roberts, "Simplified characterization of uniaxial and biaxial nonlinear optical crystals: a plea for standardization of nomenclature and conventions," IEEE J. Quantum Electron. **28**, 2057–2074 (1992).
35. T. Skauli, P. S. Kuo, K. L. Vodopyanov, T. J. Pinguet, O. Levi, L. A. Eyres, J. S. Harris, M. M. Fejer, B. Gerard, L. Becouarn, and E. Lallier, "Improved dispersion relations for GaAs and applications to nonlinear optics," J. Appl. Phys. **94**, 6447–6455 (2003).
36. M. M. Fejer, G. A. Magel, D. H. Jundt, and R. L. Byer, "Quasi-phase-matched 2nd harmonic-generation: tuning and tolerances," IEEE J. Quantum Electron. **28**, 2631–2654 (1992).
37. R. W. Boyd, *Nonlinear Optics* (Academic, 2008).
38. D. Bamford, Dr., Physical Sciences Inc., Pleasanton, CA (personal communication, 2016).
39. B. Y. Gu, B. Z. Dong, Y. Zhang, and G. Z. Yang, "Enhanced harmonic generation in aperiodic optical superlattices," Appl. Phys. Lett. **75**, 2175–2177 (1999).
40. J. Y. Lai, Y. J. Liu, H. Y. Wu, Y. H. Chen, and S. D. Yang, "Engineered multiwavelength conversion using nonperiodic optical superlattice optimized by genetic algorithm," Opt. Express **18**, 5328–5337 (2010).